Combined Spectroscopic and Theoretical Study of Narrow Band Gap Heterocyclic Co-oligomers Containing Alternating Aromatic Donor and *o*-Quinoid Acceptor Units

Mari Carmen Ruiz Delgado,[†] Víctor Hernández,[†] Juan T. López Navarrete,*[,†] Shoji Tanaka,[‡] and Yoshiro Yamashita[§]

Departamento de Química Física, Facultad de Ciencias, Universidad de Málaga, 29071-Málaga, Spain, Department of Structural Molecular Science, The Graduate University for Advanced Studies, and Institute for Molecular Science, Myodaiji, Okazaki 444, Japan, and Department of Electronic Chemistry, Interdisciplinary Graduate School of Science and Engineering, Tokyo Institute of Technology, 4259 Nagatsuta, Midori-ku, Yokohama 226-8502, Japan

Received: October 31, 2003

In this paper we analyze, with the help of density-functional theory calculations, the relationship between the molecular structure and the optical and vibrational properties of two narrow band gap π-conjugated co-oligomers containing an alternating sequence of aromatic donor and *o*-quinoid acceptor units. The optimized molecular geometries of these co-oligomers reveal that short inter-ring S···N contacts occur in their minimum-energy structure between the two types of constituiting units and that the resulting rigid coplanar arrangement of the rings enhances the degree of π conjugation and lowers the band gap.

I. Introduction

Much attention has been paid over the past few years in the field of materials science to the development of narrow band gap π-conjugated polymers (with E_g values < 1 eV) since this should lead, among other technologically interesting physical properties, to intrinsic electrical conductivity. The synthetic principles for lowering the band gap have been reviewed by Roncali.[1] A reduction of the band gap of conjugated polymers can be accomplished, among other ways, by minimizing the bond-length alternation (BLA) and by reducing the energy difference between aromatic and quinoid canonical structures such as in the case of polyisothionaphthene and soluble derivatives.[2] One successful strategy to achieve narrow band gap π-conjugated systems follows the pioneering work by Havinga and co-workers[3,4] and involves the alternation of electron-rich (donor, D) and electron-deficient (acceptor, A) units along the same conjugated chain. Several examples have been reported describing the electrochemical preparation of narrow band gap polymers consisting of an alternating sequence of an electron-withdrawing moiety such as 2,1,3-benzothiadiazole, thieno[3,4-*b*]pyrazine, benzo[1,2-*c*,4,5-*c*′]bis[1,2,5]thiadiazole, or [1,2,5]thiadiazolo[3,4-*g*]quinoxaline and an electron-releasing bithiophene or *N*,*N*′-dimethylbipyrrole group. These poly(D−A) systems exhibit optical band gaps as low as 0.5 eV.[5−8]

Co-oligomers made up from aromatic donor and *o*-quinoid acceptor heterocycles are highly polarized and should have small HOMO−LUMO gaps, thus leading to interesting properties such as absorption in the near-infrared region, nonlinear optical properties, amphoteric redox behavior, and single-component electrical conductivity.[9] These highly polarized systems have several advantages to afford organic conductors. First, intermolecular interactions can be enhanced by electrostatic interactions, which increase dimensionality in the complexes and suppress metal−insulator transitions. Second, intermolecular charge-transfer interactions are expected to occur for these donor−acceptor systems, which may be useful for crystal engineering. Third, π-extended systems have reduced on-site Coulomb repulsions, which is among the important requirements for the design of molecular organic conductors. Highly polarized co-oligomers also have low excitation energies, and interesting optical properties such as nonlinear optical responses could be expected. Finally, when the electron-donating and -accepting abilities of the various constituiting heterocycles are balanced, the compounds show amphoteric electrochemical properties.

Vis−NIR electronic absorption, IR, and Raman spectroscopies have been used since the discovery of the electrically conducting polymers to characterize many different classes of π-conjugated oligomers and polymers; and among them, Raman spectroscopy has been shown to be of great help in (i) estimating the degree of π conjugation in the neutral state,[10−12] (ii) characterizing different types of conjugational defects in doped materials,[13] and (iii) analyzing the efficiency of the intramolecular charge transfer in push−pull π-conjugated systems.[14,15] The appearance of only a few and overwhelmingly strong Raman bands, even for systems with complex chemical structures, is a direct consequence, on the basis of the effective conjugation coordinate (ECC) theory,[16] of the existence of a rather effective electron−phonon coupling over the whole quasi-one-dimensional π-conjugated backbone. In aromatic and heteroaromatic polyconjugated systems, the so-termed *collective ECC vibrational coordinate* has the analytic form of a linear combination of ring C═C/C−C stretchings which points in the direction from the benzenoid structure (usually that of the ground state) to the quinonoid structure (that corresponding to the electronically excited state or the doped species). ECC theory states that upon increasing conjugation length (CL), totally symmetric normal modes of the neutral system involved in the molecular dynamics of the ECC coordinate (namely, those that

* Author to whom correspondence may be addressed. E-mail: teodomiro@uma.es.
[†] Universidad de Málaga.
[‡] The Graduate University for Advanced Studies and Insitute for Molecular Science.
[§] Tokyo Institute of Technology.

10.1021/jp0312262 CCC: $27.50
Published on Web 02/03/2004

give rise to the few and rather strong Raman bands experimentally observed) undergo sizable dispersions both in frequency and intensity. Thus, changes in the peak positions and intensities of the Raman bands upon chain elongation are particularly useful in evaluating the *mean CL* along the members of a given series of neutral oligomers. On the other hand, when conjugated oligomers and, in particular, aromatic oligothiophenes become oxidized (either chemically or electrochemically) or photoexcited, typically, quinonoid structures are created.[17] These structural modifications also induce a significant redshift of the Raman bands associated to the π-conjugated path (due to the softening of the corresponding C═C bonds). The evolution of the Raman spectral profile between the neutral and the different doped states is a useful tool for elucidating the type of charged carriers created upon oxidation.[10−13]

In this work, we focus on the electronic and vibrational (infrared and Raman spectra) of two narrow band gap π-conjugated mixed trimers containing an *o*-quinoid electron-acceptor moiety (i.e., thieno[3,4-*b*]pyrazine or thieno[3,4-*c*][1,2,5]-thiadiazole) endowed by two thienyl rings. In particular, Raman features will allow us to assess useful information about the conjugational properties of these two co-oligomers in relation to the intramolecular charge transfer from the donor to the acceptor units. Density-functional theory (DFT) calculations will be also performed as a guide for the analysis of the electronic and vibrational spectra and to derive relevant molecular parameters such as bond lengths and angles, molecular orbital (MO) topologies, and atomic charge distribution in neutral state.

II. Experimental and Theoretical Details

UV−vis absorption spectra were recorded for each trimer in CH_2Cl_2, dioxane, DMSO, and *N*,*N*-dimethylformamide solutions (supplied by Aldrich with analytical grade) on a Perkin-Elmer Lambda 19 spectrometer. Fourier transform infrared absorption (FTIR) spectra were recorded on a Bruker Equinox 55 spectrometer. Compounds were ground to a powder and pressed in a KBr pellet. Spectra were collected with a spectral resolution of 2 cm^{-1}, and the mean of 50 scans was obtained. Interference from atmospheric water vapor was minimized by purging the instrument with dry argon prior to data collection. FT Raman spectra were collected on a Bruker FRA106/S apparatus and a Nd−YAG laser source (λ_{exc} = 1064 nm) in a backscattering configuration. The operating power for the exciting laser radiation was kept to 100 mW in all experiments. Samples were analyzed as pure solids in sealed capillaries. Typically, 1000 scans with a spectral resolution of 2 cm^{-1} were averaged to optimize the signal−noise ratio.

DFT calculations were carried out by means of the Gaussian 98 program[18] running on a SGI Origin 2000 supercomputer. We used the Becke's three-parameter exchange functional combined with the LYP correlation functional (B3LYP).[19] It has already been shown that the B3LYP functional yields similar geometries for medium-sized molecules as MP2 calculations do with the same basis sets.[20,21] Moreover, DFT force fields calculated by using the B3LYP functional yield infrared spectra in very good agreement with experiments.[22,23] We also made use of the standard 6-31G** basis set.[24] Optimal geometries were determined on isolated entities in the vacuum. All geometrical parameters were allowed to vary independently apart from planarity of the rings. On the resulting ground-state optimized geometries, harmonic vibrational frequencies and infrared and Raman intensities were calculated analytically with the B3LYP functional.

We used the often-practiced adjustment of theoretical force fields in which frequencies are uniformly scaled down by a factor of 0.96, as recommended by Scott and Radom.[22] This scaling procedure is often accurate enough to disentangle serious experimental misassignments. All quoted vibrational frequencies quoted along the paper thus correspond to the scaled values. Theoretical spectra were obtained by convoluting scaled frequencies with Gaussian functions (10 cm^{-1} width at the half height). The relative heights of the Gaussians were determined from the theoretical Raman scattering activities.

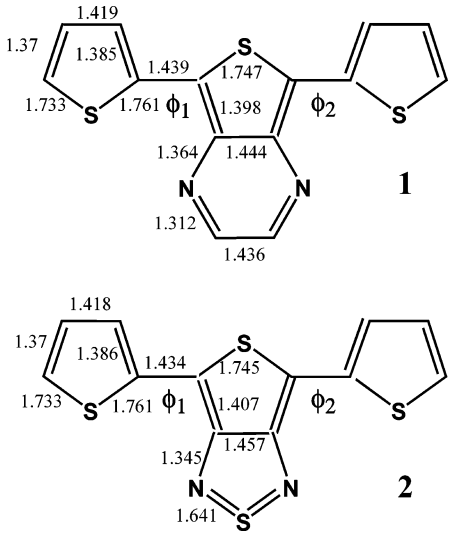

Figure 1. Selected DFT//B3LYP/6-31G**-optimized bond distances of **1** and **2**.

Calculations of gas-phase barriers to internal rotation were done by fixing the two torsion dihedral angles, ϕ_1 and ϕ_2 (see Figure 1), between the outermost and the central rings at selected values of 0 (all-syn conformation), 30, 60, 90, 120, 150, and 180° (all-anti conformation), so that both donor units rotate clockwise with respect to the acceptor moiety and they lay always in the same plane. Energy differences are always relative to the corresponding absolute minimum conformation. All geometrical parameters were completely optimized along the torsional potential curve to account for the molecular relaxation, yielding a physically meaningful picture of nonrigid rotation.

Vertical electronic excitation energies were computed by using the time-dependent DFT (TDDFT) approach.[25,26] The twenty lowest-energy electronic excited states were computed for the two molecules. Numerical applications reported so far indicated that TDDFT employing current exchange-correlation functionals performs significantly better than HF-based single excitation theories for the low-lying valence excited states of both closed-shell and open-shell molecules.[27] TDDFT calculations were carried out using the B3LYP functional and the 6-31G** basis set on the previouly optimized molecular geometries obtained at the same level of calculation.

The synthesis of 5,7-dithien-2-ylthieno[3,4-*b*]pyrazine (hereafter referred to as **1**) has been reported elsewhere,[6,26] while the synthetic route to afford the second mixed trimer subject of research in this work, 4,6-dithien-2-ylthieno[3,4-*c*][1,2,5]-thiadiazole (**2**), is shown in Scheme 1.

A mixture of 3′,4′-diamino-2,2′,5′,2″-terthiophene **3** (1.67 g, 5.99 mmol), thionylanyline (1.6 g, 12 mmol), and chlorotrimethylsilane (4.5 g, 41 mmol) was stirred in pyridine (30 mL) at room temperature for 1 h. The mixture was poured into dichloromethane (400 mL). The solution was then washed with 1 N HCl (240 mL × 2) to remove the pyridine and dried over Na_2SO_4. After removal of the solvent under reduced pressure at room temperature, recrystallization from hexane afforded 1.72

SCHEME 1

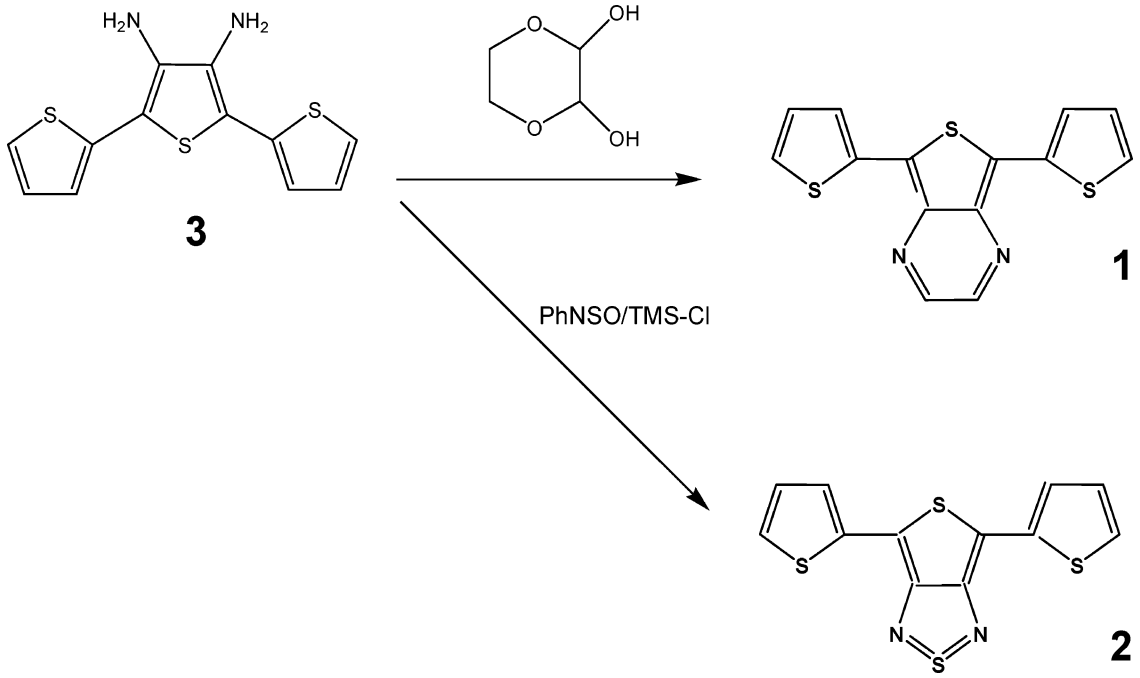

g of **2** as blue needles. Yield 94%; mp 157−158 °C. ^{1}H NMR (400 MHz, CD_2Cl_2) δ: 7.55 (d, *J* 3.7 Hz, 2H), 7.32 (d, *J* 4.9 Hz, 2H), 7.09 (dd, *J* 4.9, 3.7 Hz, 2H); ^{13}C NMR (100 MHz, CD_2Cl_2) δ 156.2, 134.9, 128.2, 125.4, 124.3, 112.4; UV−vis λ_{max}/nm (CH_2Cl_2) 618.0 (log ϵ 4.04), 360.5 (log ϵ 4.28), 307.5 (log ϵ 4.38); IR (KBr) ν_{max} cm^{-1} 3102, 3072, 1524, 1488, 1428, 1406, 1367, 1224, 1143, 1013, 847, 832, 708, 686, 672, 498, 486; MS (EI) *m*/*z* 306 (M^+, 100), 153 (24), 127 (33). Anal. Calcd for $C_{12}H_6N_2S_4$: C, 47.04; H, 1.97; N, 9.14. Found: C, 46.85; H, 1.96; N, 9.07.

III. Results and Discussion

A. Optimized Geometries. The molecular geometries of **1** and **2** were optimized, at the DFT//B3LYP/6-31G** level, without imposing any constraint for selected values of the two inter-ring dihedral angles. For the two compounds, the fully coplanar arrangements of the three constituting rings are predicted as the most stable gas-phase structures. As for **1**, the all-anti conformation is predicted to be 1.22 kcal/mol more stable than the all-syn one, showing the compound a potential barrier to internal rotation of 9.87 kcal/mol for $\phi_1 = \phi_2 = 90°$ (i.e., the molecular arrangement less favorable to the π conjugation). On the other hand, for **2**, the all-anti and all-syn conformations are also found to be the most preferred arrangements, and they display nearly the same energy values, whereas in this case the potential barrier to internal rotation amounts to 9.71 kcal/mol for $\phi_1 = \phi_2 = 90°$. For comparison purposes, we have performed similar calculations on various rotamers of unsubstituted terthiophene. For the later compound, the conformer with $\phi_1 = \phi_2 \approx 30°$ from the all-anti coplanar conformation is found to be the lowest-energy gas-phase structure, while the DFT//B3LYP/6-31G** barrier to internal rotation does not exceed 6.3 kcal/mol. The larger energy barriers to internal rotation for **1** and **2** with respect to terthiophene can be attributed to (i) the increased π conjugation in these D−A−D structures (and the consequent strengthening of the inter-ring CC bonds), (ii) the closed-shell interactions between heretoatoms of adjacent rings for the all-anti conformation, and (iii) the intramolecular hydrogen bonds between the donor and acceptor units for the all-syn conformation of **2**. Since the all-anti arrangement is the most favorable to the π conjugation and it is commonly found in most of oligothienyl materials, in what follows, calculations for **1** and **2** will be discussed by assuming this molecular structure.

As aforementioned, quite short inter-ring contacts between sulfur atoms of the outermost thienyl rings and nitrogen atoms of the central electron-withdrawing moiety (namely, of 3.04 Å for **1** and 3.19 Å for **2**, smaller than the sum, 3.35 Å, of the van der Waals S−N radii) are among the reasons for such a preferred coplanar molecular conformation. Geometrical features predicted by DFT calculations on isolated entities are in agreement with the close intramolecular distances between heteroatoms of successive α-linked units and the low values of dihedral angles between the end thienyl rings and various kinds of *o*-quinoid acceptor moieties as previously revealed by the X-ray analyses of some related narrow band gap mixed co-oligomers (for which steric hindrance to intramolecular rotation was almost negligible or absent).[6] In some cases, strong intermolecular interactions also based on short heteroatom contacts help to improve the solid-state structural order and to enhance the charge transport between adjacent molecules.

Main theoretical bond lengths for the all-anti conformations of **1** and **2** are sketched in Figure 1. In both cases, the shortest carbon−carbon (CC) length of the whole π-conjugated spine corresponds to the outermost C_α=C_β double bonds of the end-capping thienyl rings (≈1.370 Å). We also notice that the thienyl donor units display almost the same geometry for **1** and **2**, the C_β−C_β and the inner C_α=C_β distances (whose optimized values are 1.418 and 1.386 Å, respectively), are somewhat different from those previously found, at the same level of theory, for the outer rings of an α-linked terthiophene with the two β positions of the central ring substituted by butyl side chains (i.e., 1.423 and 1.380 Å).[29] These geometrical changes suggest a certain increase of the overall π conjugation in going from the homogeneous oligothiophenes to this type of mixed cooligomers. The optimized values for the inter-ring C_α−C_α bond distances of **1** and **2** give further support to this conclusion, since in the two cases they are shorter by around 0.02 Å than

TABLE 1: UV−vis Absorption Maxima (λ_{Max}) of 1 and 2 in Dichloromethane, Dioxane, DMSO, and *N,N*-dimethylformamide Solutions

compound	CH_2Cl_2[a]	dioxane[a]	DMSO[a]	DMF[a]
1	528	528	528	526
2	618	614	622	620

[a] λ_{max} values in nm.

in the aforementioned α-linked terthiophene (referred to as HT_3H in Table 1 of ref 29). Main geometrical differences between **1** and **2**, on one hand, and the HT_3H terthiophene taken as a reference, on the other hand, occur for the innermost thienyl ring. In this regard, we observe that both the inner C_α═C_β and C_β—C_β bonds are longer than those of HT_3H, 1.398 and 1.444 Å, respectively, for **1** and 1.407 and 1.457 Å for **2** vs 1.385 and 1.441 Å for HT_3H. A feasible reason for this could be a partial loss of π electron density over this thienyl unit due to the electron-withdrawing ability of the fused pyrazine and thiadiazole rings. The optimized values for the C═S bonds of the thiadiazole ring of **2** (1.641 Å) are in agreement with their double-bond character, while the C—S distances of the innermost thienyl unit (whose values are quite similar for the two trimers, 1.747 Å for **1** and 1.745 Å for **2** vs 1.751 Å in HT_3H) are rather less affected by the electron-withdrawing ability of the fused rings.

It has been hypothesized that the bond-length alternation (BLA) (i.e., the difference between average lengths of carbon−carbon single and double bonds in a π-conjugated backbone) is a useful parameter to consider when establishing structure−property relationships for polyconjugated molecules.[30−33] The degree of BLA has been used as a structural parameter in interpreting electronic spectra of many classes of donor/acceptor polyconjugated oligomers and polymers.[34] The degree of BLA, calculated as the difference between average lengths of the C—C and C═C bonds of the π-conjugated path amounts to +0.043 Å for **1** and **2**, a value similar to that derived from the DFT//B3LYP/6-31G** molecular geometry optimization of 3′,4′-dibutyl-5,5″-dinitro-2,2′,5′,2″-terthiophene (i.e., a poor π electron system termed as $NO_2T_3NO_2$ in ref 29), for which the molecular structure of the π-conjugated backbone changes from the typical aromatic pattern of HT_3H (BLA = 0.063 Å) to a partially quinonoid-like pattern in which the BLA values are drastically reduced. Similar BLA values to those of **1** and **2**, of around 0.045 Å, were also calculated for some asymmetrically end-capped terthiophene having a pronounced push−pull character, such as 3′,4′-dibutyl-5-nitro-5″-phenyl-2,2′,5′,2″-terthiophene and 3′,4′-Dibutyl-5-nitro-5″-bromo-2,2′,5′,2″-terthiophene.[29]

The B3LYP/6-31G** natural bond orbital atomic charges for **1** and **2** are plotted in Figure 2. Useful information can be gathered from the overall sum of all the atomic charges on each ring (i.e., from the net charges located over each alternating donor/acceptor unit of the oligomeric chain). As for **1**, the net charges on the donor thienyl rings and the central thieno[3,4-*b*]pyrazine acceptor moiety amount +0.029 and −0.057 e, respectively, and the corresponding values are nearly the same for **2**, +0.027 and −0.054 e. In both cases, the negative charge over the central *o*-quinoid moiety is mainly storaged either on the [3,4-*b*]pyrazine or the [3,4-*c*][1,2,5]thiadiazole-fused rings. Thus, the overall charges on these molecular domains (without taking into consideration the positive atomic charges of around +0.110 e on the C_β atoms of the central thienyl ring) amount to −0.360 e for **1** and −0.312 e for **2**. We also observe that the thiadiazole-fused ring of **2** is largely polarized since its sulfur

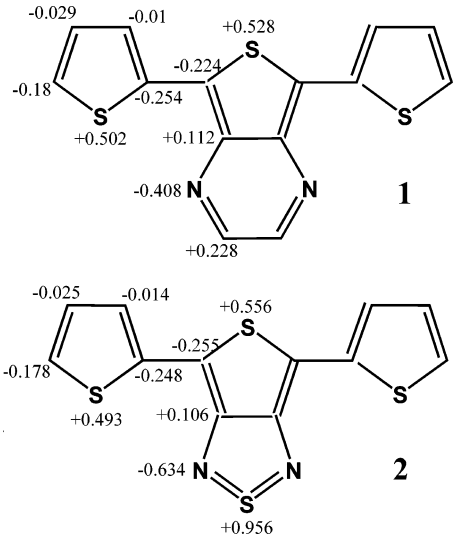

Figure 2. Natural bond orbital atomic charges (with hydrogens summed into heavy atoms) for **1** and **2**, as deduced from their optimized DFT//B3LYP/6-31G** molecular geometries.

atom bears a positive charge of +0.956 e, whereas the two adjacent nitrogen atoms are negatively charged by −0.634 e.

B. Electronic Spectra. Table 1 lists the UV−vis absorption maxima (λ_{max}) of **1** and **2** in a variety of solvents with different polarities, while Figure 3 displays the whole UV−vis absorption spectral profile of **1** and **2** in CH_2Cl_2 solution. The two compounds show similar spectral patterns with three main bands, 238, 298−346 (double-peak structure), and 528 nm for **1**; and 236, 308−360 (double-peak structure), and 618 nm for **2** (values for dichloromethane solutions). The lowest-energy absorption, with maxima at 528 nm for **1** and at 618 nm for **2,** largely shifts downward with respect to the related absorptions at 351 and 415 nm for the unsubstituted thieno[3,4-*b*]pyrazine and thieno-[3,4-*c*][1,2,5]thiadiazole electron-withdrawing units,[35] respectively, and at 350 nm for the fully aromatic α-terthiophene. The optical absorption data indicate that these two co-oligomers are characterized by a small HOMO−LUMO separation (particularly in the case of **2**), which could be the result of a significant degree of intramolecular charge transfer from the end-capping thienyl donor rings to the central electron acceptor *o*-quinoid unit.

To investigate the nature of the electronic transitions that give rise to the absorption bands observed experimentally, the lowest-energy electronic excited states of **1** and **2** were calculated at the B3LYP/6-31G** level using the TDDFT approach on the optimized molecular geometries depicted in Figure 1.

Theoretical calculations predict the appearance of three strong electronic transitions in the UV−vis region (see Table 2). The bands measured, in dichloromethane solution, at 2.35 eV for **1** and at 2.01 eV for **2** are due to the $1^1A_1 \rightarrow 1^1B_2$ excitation to the first singlet excited electronic state, which is computed at 2.08 eV for **1** (with a oscillator strength, *f*, of 0.24) and at 1.71 eV for **2** ($f = 0.21$). This vertical transition is mainly described by a one-electron excitation from the HOMO to the LUMO. Experimental energies for the $\pi-\pi^*$ transition in the two mixed trimers are slightly underestimated, by around 0.3 eV, by TDDFT model chemistry, which however nicely accounts for the observed redshift in passing from **1** to **2**. The atomic orbital composition of the frontier molecular orbitals obtained for **1** is sketched in Figure 4a. For the two molecules, the HOMO is of a π nature and is delocalized over the whole CC backbone (with a small contribution from the N═C bonds of the fused pyrazine ring in **1** and of the nitrogen atoms of the thiadiaziole ring in

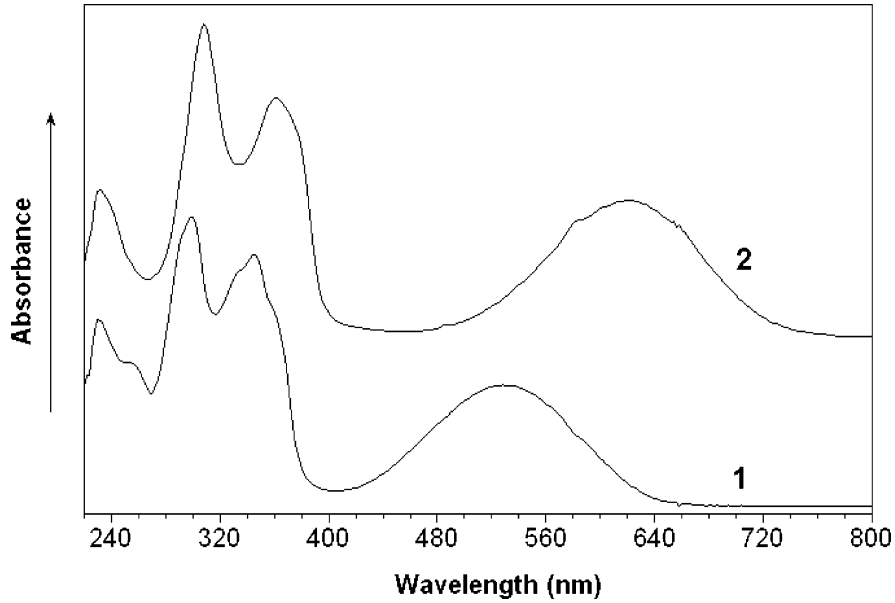

Figure 3. UV−vis absorption spectra of **1** and **2** in dichloromethane solution.

TABLE 2: Main TDDFT//B3LYP/6-31G Vertical Electronic Transitions for 1 and 2 in the UV−vis Spectral Region**

1			2		
exp[a]	TDDFT//B3LYP-(6-31G*)[a]	description	exp[a]	TDDFT//B3LYP-(6-31G*)[a]	description
2.35	2.08 ($f = 0.24$)	H → L	2.01	1.71 ($f = 0.24$)	H → L
3.58	3.58 ($f = 0.50$)	H → L + 1	3.44	3.42 ($f = 0.57$)	H → L+1
4.16	4.41 ($f = 0.28$)	H −5 → L H → L + 2	4.03	4.35 ($f = 0.22$)	H −4 → L H → L + 3
5.21	5.07 ($f = 0.02$)	H −1 → L + 1 H → L + 4	5.25	5.28 ($f = 0.03$)	H −2 → L + 1 H → L + 9

[a] Values in eV.

2). By contrast, the LUMO is almost exclusively concentrated on the central electron-withdrawing moiety, contrary to what is commonly found in usual aromatic oligothiophenes for which both HOMO and LUMO spread over the whole π-conjugated path (please, compare the related frontier MO topologies for HT_3H shown in Figure 4b). Consequently, the HOMO → LUMO transition in these narrow band gap systems implies certain electron-density transfer from the aromatic-like donor thienyl end rings to the more quinoid-like molecular domain, the central electron-acceptor unit. Moreover, the HOMO and LUMO topologies show certain overlap, which is a prerequisite to allow for an effective intramolecular charge transfer. Thus, on the basis of the theoretical TDDFT results, the absorptions at 528 nm for **1** and 618 nm for **2** correspond to a charge-transfer absorption band.

One could in principle think that a lowering of the band gap is mainly a consequence of the large stabilization of the LUMO, due to the strong electron-acceptor ability of the central *o*-quinoid ring. It has already been shown that, upon the attachment of electron-withdrawing groups at the end α positions of linear α-linked π-conjugated chains, the relative energies of the HOMO and LUMO move toward lower values with respect to the unsubstituted system, affecting the LUMO more than the HOMO and thus lowering the band gap.[29,36] However, DFT calculations for **1** and **2** reveal a different trend, insertion of an *o*-quinoid thieno[3,4-*c*][1,2,5]thiadiazole or thieno[3,4-*b*]pyrazine electron-acceptor moiety between two donor thiophene rings stabilizes the LUMO but destabilizes the HOMO in a similar extent, thus causing a large reduction of the band gap (Figure 5).

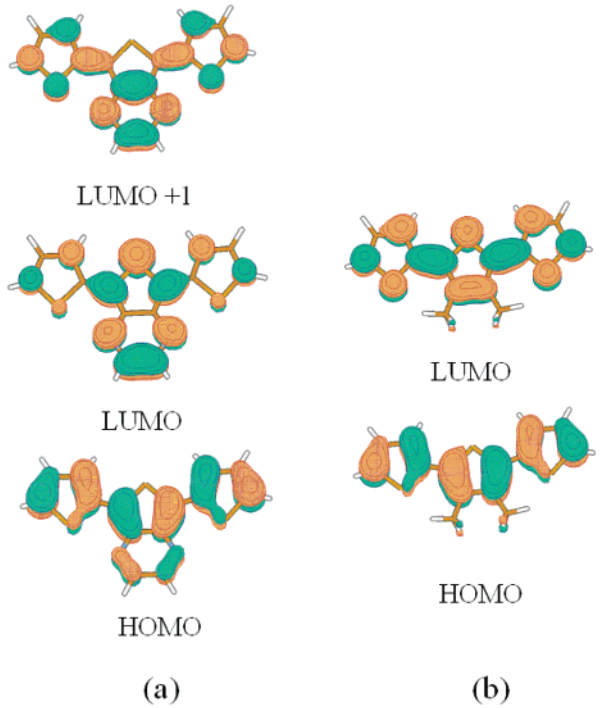

Figure 4. Electronic density contours (0.03 e/bohr^3) calculated for the frontier molecular orbitals of the (a) **1** and (b) the model HT_3H terthiophene.

Calculations predict that the strong absorptions in the visible region of **1** (3.58 eV) and **2** (3.44 eV) arise, as for **1**, from the

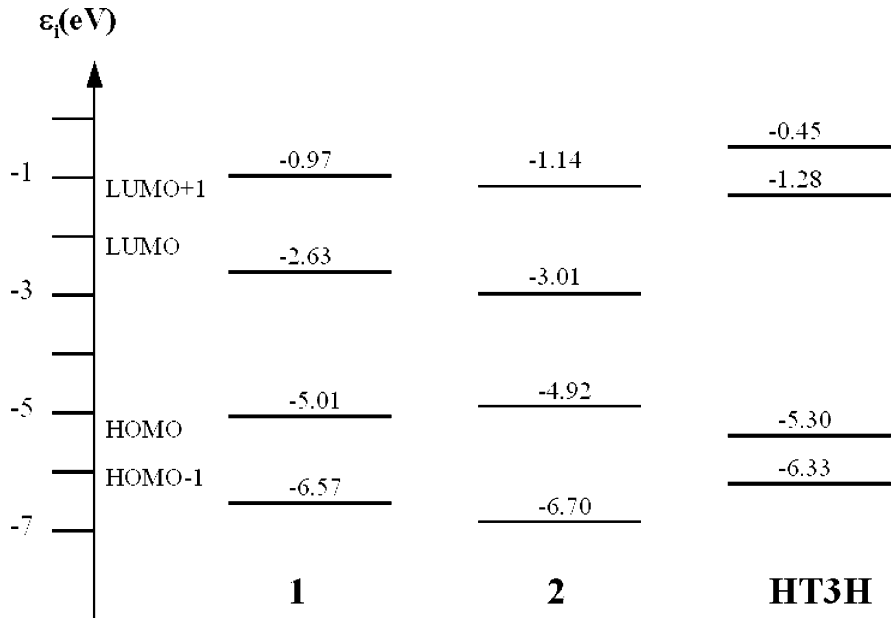

Figure 5. B3LYP/6-31G** one-electron energies (ϵ_i) diagram of the band gap region around the frontiers molecular orbitals of **1** and **2** and the model HT_3H terthiophene taken as reference.

$1^1A_1 \rightarrow 2^1B_2$ transition (3.58 eV, $f = 0.50$) and, as for **2**, from the $1^1A_1 \rightarrow 3^1B_2$ transition (3.42 eV, $f = 0.57$). For both compounds, this transition can be described as the HOMO → LUMO + 1 excitation; the topologies of these HOMO and LUMO + 1 orbitals are quite similar, respectively, to the HOMO and LUMO which give rise to the strong $\pi-\pi^*$ absorption band in homogeneous α-linked oligothiophenes (please, compare parts a and b of Figure 4), the only difference being a partial contribution by the pyrazine or thiadiazole-fused ring to the LUMO + 1 orbital. We also see that the LUMO + 1 of **1** and **2** are slightly destabilized, by less than 0.3 eV, with respect to the LUMO of HT_3H (Figure 5). However, the concomitant destabilization of the HOMO orbital in **1** and **2** by around 1.30−1.40 eV with respect to HT_3H makes the electronic transition between the aforementioned occupied and unoccupied orbitals to have similar excitation energies for the three molecules. Thus, the strong visible absorption of these mixed trimers ≈ 350 nm is to be correlated with the $\pi-\pi^*$ absorption band near 350 nm for the fully aromatic nonpolar α-terthiophene.

The absorptions experimentally measured at 4.16 and 4.03 eV for **1** and **2**, respectively, must be theoretically correlated to the $1^1A_1 \rightarrow 5^1A_1$ transition, which is calculated for **1** at 4.41 eV ($f = 0.28$) and for **2** at 4.35 eV ($f = 0.22$). This electronic transition can be mainly described, as for **1**, to a combination of the HOMO − 5 → LUMO and HOMO → LUMO + 2 excitations, whereas for **2**, it is due to a combination of the HOMO − 4 → LUMO and HOMO → LUMO + 3 excitations. The multiconfigurational character of these transitions is due to the near degeneracy of the one-electron excitations involved. The HOMO − 5 → LUMO (**1**) and HOMO − 4 → LUMO (**2**) excitations are to be assigned, following the theoretical B3LYP/6-31G** description of the optical absorption spectra of these mixed trimers, to characteristic bands of the *o*-quinoid thieno-[3,4-*c*][1,2,5]thiadiazole and thieno[3,4-*b*]pyrazine central units.

Finally, the weak ultraviolet absorptions at 5.21 (**1**) and 5.25 eV (**2**) are computed as due to the $1^1A_1 \rightarrow 6^1A_1$ transition (5.07 eV, $f = 0.02$) for **1** and as the $1^1A_1 \rightarrow 7^1A_1$ transition (5.28 eV, $f = 0.03$) for **2**. This electronic transition can be mainly described for **1** as being due to a combination of the HOMO − 1 → LUMO + 1 and HOMO → LUMO + 4 one-electron excitations, whereas for **2**, it arises from a combination of the HOMO − 2 → LUMO + 1 and HOMO → LUMO + 9 excitations. Of them, the HOMO − 1 → LUMO + 1 (**1**) and HOMO − 2 → LUMO + 1 (**2**) excitations imply a low electron density transfer from the donor thienyl end rings to the pyrazine or thiadiazole-fused rings.

C. Vibrational Spectra. Figure 6 shows the infrared spectra of **1** and **2**, whereas the comparison between the FT Raman spectra and the corresponding B3LYP/6-31G** spectral profiles of **1** and **2** are plotted in Figures7 and 8, respectively. As a first observation, we notice that the IR and Raman spectra of each compound are complementary, in the sense that what is strong in the IR is weak in the Raman and vice versa. This is the usual spectroscopic behavior of the unsubstituted and symmetrically end-capped oligothiophenes (i.e., in nonpolar π-conjugated systems).[8−10] On the contrary, when the end α and ω positions of a π-conjugated oligomer are attached to a donor and an acceptor group to afford a push−pull chromophore with an effective intramolecular charge transfer, several vibrational normal modes become strongly active both in the infrared and Raman spectra. This observation has been previously reported for push−pull oligoenes and oligothiophenes.[29,37,38]

Although the theoretical B3LYP/6-31G** analysis of the UV−vis absorption spectra of **1** and **2** has revealed the occurrence of a partial electron density transfer from the thienyl rings to the central *o*-quinoid unit, the symmetric structure of these narrow band gap mixed co-oligomers makes this intramolecular charge-transfer process to give rise neither to a large molecular dipole moment nor to extra-large IR intensities of the skeletal ν(C=C) stretching vibrations, contrarily to what was found for the class of the asymmetrical-substituted push−pull π-conjugated chromophores. In the latter case, relative IR intensities of bands appearing in the1600−1000 cm^{-1} spectral region (namely, those associated to skeletal vibrations of the π-conjugated backbone) are comparatively very much stronger than those recorded for the nonpolar oligothiophenes (for which the strongest IR bands are by far those appearing at ∼800 and/or 670 cm^{-1} and due to out-of-plane γ(CH) deformations).

The precise assignment of each infrared absorption of **1** and **2** to particular vibrations is beyond the scope of our analysis. We will restrict our discussion to the more relevant observations of general validity for this class of molecular materials. Both **1**

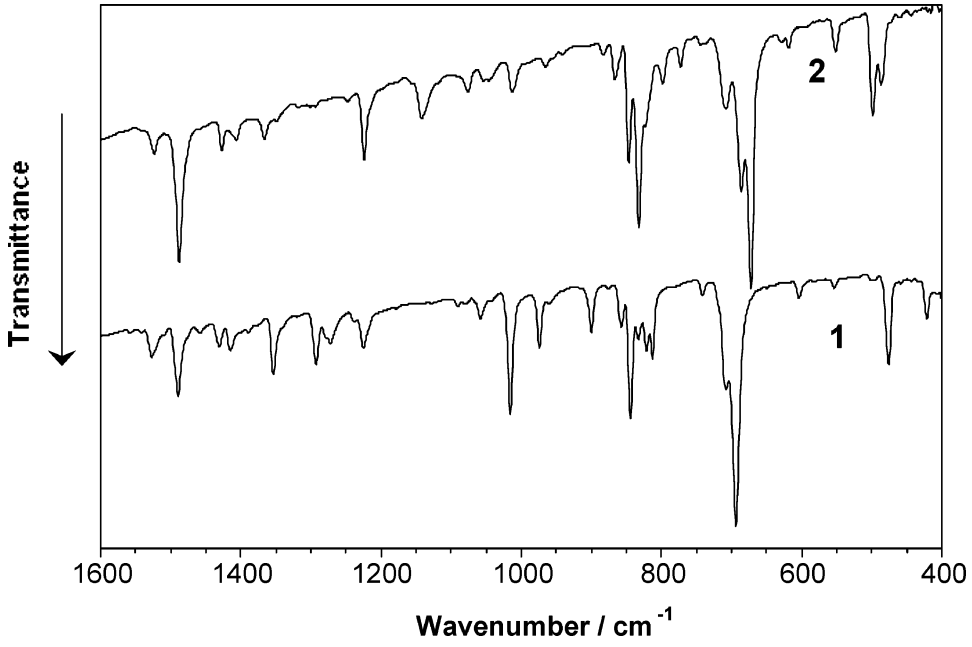

Figure 6. FTIR spectra of **1** and **2** in the form of pressed KBr pellets over the 1600−400 cm^{-1} spectral region.

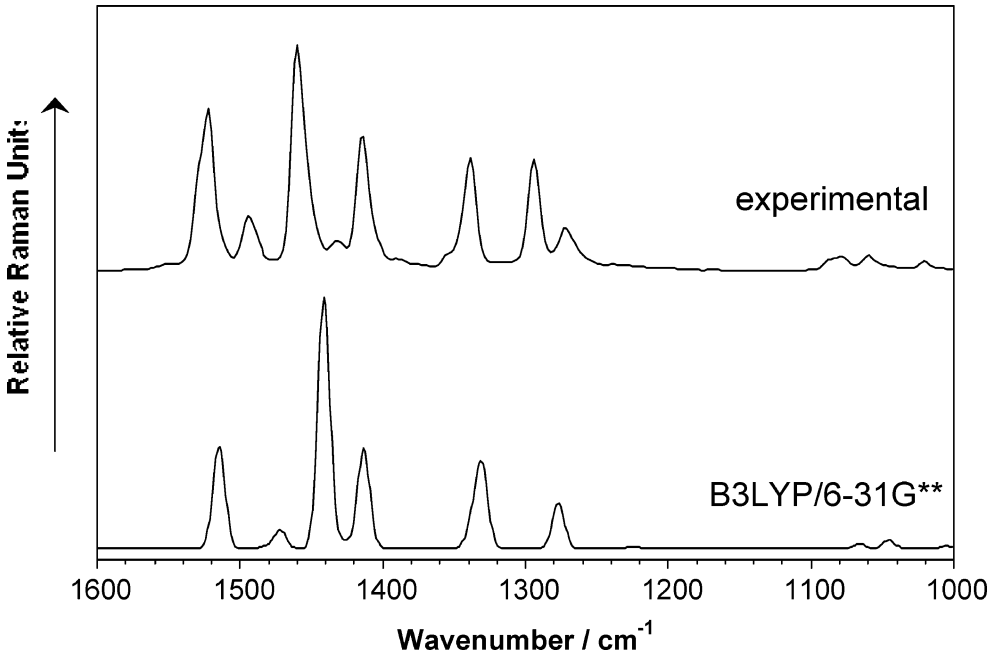

Figure 7. Comparison between the experimental FT Raman spectrum of **1** and the theoretical B3LYP/6-31G** spectrum over the 1600−1000 cm^{-1} spectral region.

and **2** display a strong and structured IR feature around 670−690 cm^{-1}, which is mainly due to the out-of-plane γ(CH) deformations of the hydrogens at the end α and ω positions of the π-conjugated skeleton, while the corresponding motions of hydrogens at the β positions, and various mixtures of asymmetric ν(CS) and ν(NS) stretchings of the thienyl and thiadiazole rings, are to be assigned to the 5−6 bands recorded in the 780−840 cm^{-1} spectral range (B3LYP/6-31G** vibrational eigenvectors are available upon request to the authors). We also observe that, despite their different chemical structures, the two mixed trimers display a similar spectral pattern, both in peak positions and relative intensities, in the 1600−1400 cm^{-1} frequency range: (i) the IR band at 1527 cm^{-1} (**1**) and 1523 cm^{-1} (**2**) is mainly due to the out-of-phase ν_{asym}(C═C) stretching of the outermost thienyl rings, (ii) the stronger absorption in this region, measured at 1489 cm^{-1} for **1** and 1488 $cm^{-1}$for **2**, arises from the asymmetric ν(C═C) stretching of the central *o*-quinoid unit, whereas (iii) peaks at 1431 cm^{-1} (**1**) and 1427 cm^{-1} (**2**) are to be assigned to the out-of-phase ν_{sym}(C═C) stretching of the outermost thienyl rings. The fact that the ν_{asym}(C═C) stretching vibration of the acceptor unit is measured in the two trimers at a frequency value lower than the related ν_{asym}(C═C) mode of the donor thienyl end rings agrees with a sizable softening of the C_α═C_β double bonds of the central thienyl ring with respect to the outer ones. Thus, the two IR absorptions around 1525 and 1488 cm^{-1} of **1** and **2** are related to those of unsubstituted terthiophene experimentally measured at 1497 cm^{-1}, which is due to a collective ν_{asym}(C═C) mode spreading over the whole π-conjugated backbone.[34] The "splitting" of the original vibration of the homogeneous terthiophene into two components for this class of narrow band gap mixed trimers is a consequence of the coexistence of two quite different molecular domains in

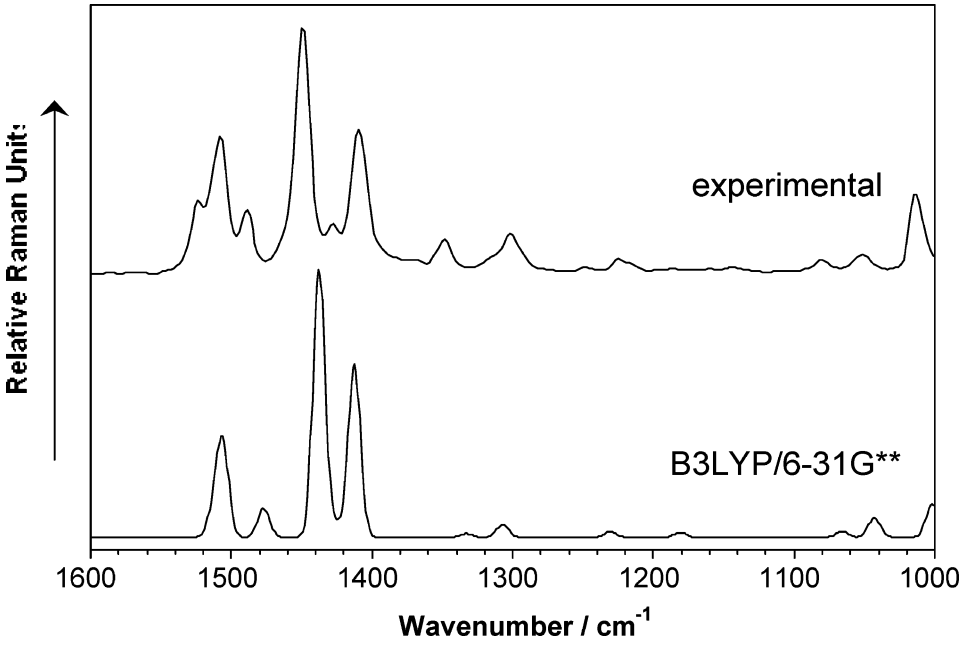

Figure 8. Comparison between the experimental FT Raman spectrum of **2** and the theoretical B3LYP/6-31G** spectrum over the 1600−1000 cm^{-1} spectral region.

TABLE 3: Assignment of the Main Infrared Absorptions of 1 and 2 with the Help of B3LYP/6-31G Vibrational Calculations**

ν_{exp} (cm^{-1})		
1	**2**	B3LYP/6-31G** theoretical assigment
1527	1523	ν_{asym}(C═C) of outermost thienyl rings
1489	1488	ν_{asym}(C═C) of central thienyl ring
1431	1427	out-of-phase ν_{sym}(C═C) of outermost thienyl rings
1354		ν_{sym}(CN) of fused pyrazine ring
1293		δ_{sym}(CH) of fused pyrazine ring
1225	1224	δ_{asym}(C_β-H) of outermost thienyl rings
	1142	out-of-phase $\nu_{inter-ring}$(C−C) + ν_{asym}(CN) of fused thiadiazole ring
1016		ν(C−C) + δ_{sym}(CH) of fused pyrazine ring
	1013	ν(C−C) + in-plane δ(CC) of fused thiadiazole ring
973		in-plane δ_{ring} of fused pyrazine ring
	847	ν_{asym}(CS) + ν_{asym}(SN)
844		ν_{asym}(CS) + in-plane δ_{ring}
	832	ν_{sym}(CS) + ν_{asym}(SN)
693	672	γ(CH) of outermost thienyl rings
475	498	γ_{ring}
	486	δ_{ring}

the same molecule: (i) the aromatic-like donor end rings and (ii) the quinoid-like central acceptor moiety.

Finally, in nonpolar oligothiophenes, the 1300−800 cm^{-1} infrared region is dominated by the appearance of the ring ν-(C_β−C_β) and inter-ring ν(C_α−$C_{\alpha'}$) skeletal stretching modes and the in-plane δ(C−H) bendings.[10] The IR absorption profiles of **1** and **2** are a little bit more complex since, among other reasons, many of the characteristic vibrations of the *o*-quinoid acceptor unit take place in this spectral range (see Table 3 for their assignment).

The current Raman spectra of **1** and **2** are reproduced by the B3LYP/6-31G** calculations with remarkable accuracy (Figures 7 and 8). We first notice that for the two mixed trimers the Raman scattering spectral profile is simpler than the IR absorption one; the strongest lines are found in the1600−1000 cm^{-1} Raman-shift spectral range (namely, most of them are associated to skeletal ν(CC) stretching modes), while almost all Raman features below this region display a rather weak intensity. Moreover, we observe that **1** and **2** show an increased number of Raman lines in comparison with unsubstituted terthiophene, the latter taken as the prototypical case for the class of nonpolar homogeneous oligothiophenes. In this regard, the three Raman lines measured for **2** near 1523, 1489, and 1429 cm^{-1} have a counterpart in the IR spectrum, whereas for unsubstituted terthiophene, the IR and Raman spectral patterns in the1600−1000-cm^{-1} frequency range were found to be fully complementary (i.e., Raman lines displayed negligible IR activity and vice versa).[39]

The overwhelming enhancement, commonly observed for the nonpolar oligothiophenes, of four characteristic Raman lines with respect to the very many Raman-active vibrations theoretically predicted by the optical selection rules was explained fifteen years ago in terms of lattice-dynamics, as mentioned in the introductory section, by assuming the existence in these quasi-one-dimensional systems of a large electron−phonon coupling.[16] These four Raman scatterings were termed as *Lines A, B, C,* and *D,* and their spectroscopic behavior is as follows: (i) Line A largely shifts downward and becomes weaker with increasing length of the π-conjugated backbone and is due to a totally symmetric in-phase ν_{asym}(C═C) stretching mainly located on the outer thienyl rings of the chain. (ii) Line B is always the strongest one of the spectrum, and its peak-position quickly meets saturation with increasing chain length; it results from a collective totally symmetric ν_{sym}(C═C) mode along which all thiophene rings of the chain vibrate in phase and with similar amplitudes. (iii) Line C displays an appreciable intensity only for α- and/or β-substituted oligothiophenes, also due to a collective totally symmetric ν_{sym}(C═C) mode along which the successive thiophene rings vibrate out-of-phase and with similar amplitudes. (iv) Finally, Line D arises from a totally symmetric in-plane δ_{sym}(C−H) bending mode, along which all hydrogens at the β positions of the π-conjugated chain vibrate fully in phase. Lines A, B, C, and D are recorded, respectively, at 1524, 1453, 1417, and 1045 cm^{-1} for unsubstituted terthiophene,[39] whereas they upshift to 1546, 1488, 1445, and 1044 cm^{-1} for α,ω-dimethyl end-capped terthiophene as a result of the strengthening of the π-conjugated path due to the inductive effects by the alkyl side-chains.[12a]

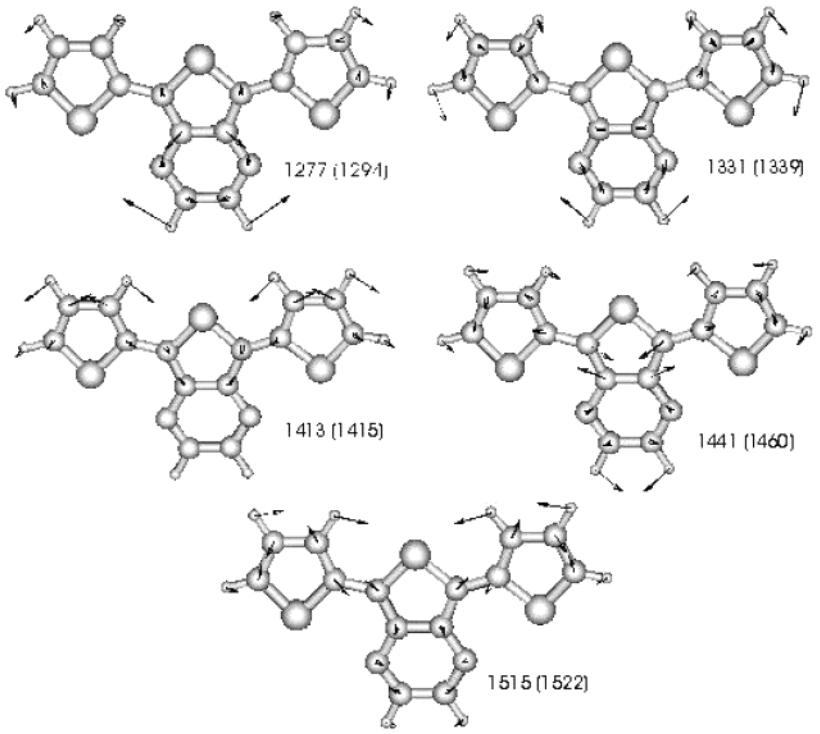

Figure 9. Selected Raman-active theoretical B3LYP/6-31G** vibrational eigenvectors for **1**. Theoretical and experimental (within parentheses) frequency values are given in cm^{-1}.

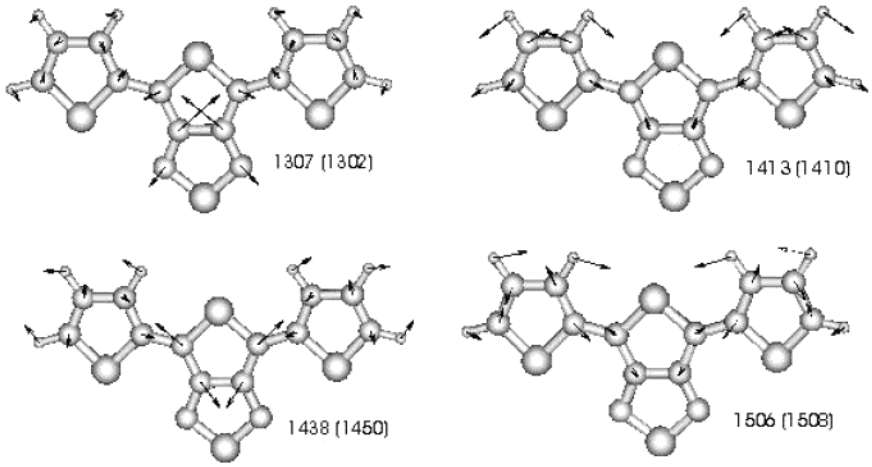

Figure 10. Selected Raman-active theoretical B3LYP/6-31G** vibrational eigenvectors for **2**. Theoretical and experimental (within parentheses) frequency values are given in cm^{-1}.

B3LYP/6-31G** vibrational calculations show that the experimental Raman scatterings at 1522, 1460, and 1415 cm^{-1} for **1** and at 1508, 1450, and 1410 cm^{-1} for **2** are to be correlated with the characteristic lines A, B, and C, respectively, of the homogeneous oligothiophenes (see eigenvectors in Figures 9 and 10). The redshift of lines A and B (i.e., 14 and 10 cm^{-1}, respectively) in passing from **1** to **2** indicates that the insertion of the *o*-quinoid thieno[3,4-*c*][1,2,5]thiadiazole acceptor unit between the two thienyl rings causes a larger softening of the π-conjugated backbone than in the 5,7-dithien-2-ylthieno[3,4-*b*] pyrazine mixed trimer, in agreement with the aforementioned UV−vis data. It is not straightforward however, for this type of narrow band gap heterocyclic co-oligomer, to assess reliable structural information only from the simple correlation of the peak positions of lines A and B between unsubstituted terthiophene, on one hand, and **1** and **2**, on the other hand, since for the latter two trimers some ν(CN) stretchings of the fused pyrazine and thiadiazole rings contribute to some extent to the eigenvectors associated to Raman lines A and B, as shown in Figures 9 and 10, whereas in homogeneous terthiophene they arise from pure skeletal ν(CC) stretching modes of the thienyl units. In this regard, we also observe that the peak positions of lines A and C in **1** are roughly coincident with those found for unsubstituted terthiophene, but line B is upshifted by 7 cm^{-1}, whereas for **2**, line B appears at nearly the same frequency as in terthiophene, but now lines A and C are downshifted by 16 and 7 cm^{-1}, respectively.

Finally, calculations show that the two Raman scatterings measured for **1** at 1339 and 1294 cm^{-1}, and whose relative intensities are similar to that of line C, are due to totally symmetric ν(CN) stretchings of the fused pyrazine ring somewhat mixed with in-plane δ(C−H) bendings both of the thienyl and pyrazine rings. As for **2**, lines at 1302 and 1014 cm^{-1} are to be assigned, respectively, to ν_{sym}(CN) stretching and an in-

plane δ(CN) bending modes, and thus both Raman scatterings are associated to specific vibrations of the thiadiazole-fused ring.

Conclusions

In summary, we have reported on the synthesis of a novel mixed co-oligomer with a donor−acceptor−donor structure to complete a previously reported series of narrow band gap heterocyclic mixed trimers built around a central *o*-quinoid electron-withdrawing moiety. We have performed DFT quantum chemical calculations on the internal torsion potentials of the two mixed trimers, which reveal the preference for the fully coplanar arrangement of the various constituting donor/acceptor units of these D−A−D cooligomers. The DFT/B3LYP/6-31G** molecular geometry optimizations performed for the all-anti conformation of the two compounds studied in this work evidence the occurrence of short intramolecular contacts between nitrogen atoms of the central acceptor moiety and sulfur atoms of the adjacent thienyl end-capping rings. The analysis of the structure of the π-conjugated backbone of each compound in terms of B3LYP/6-31G** BLA values (evaluated as the difference between the average lengths of the skeletal C−C and C═C bonds) is consistent with a partial quinonoid-like pattern. The electrostatic picture of this type of D−A−D systems in terms of equilibrium NBO atomic charges also indicates that their ground-state structure really corresponds to a charge-separated state, in which the thienyl end rings lend some electron density to the central *o*-quinoid acceptor moiety, being almost all the net negative charge of the molecule storaged either over the [3,4-*b*]pyrazine or the [3,4-*c*][1,2,5]thiadiazole-fused rings.

The two compounds show a similar optical absorption spectral pattern in the visible region, with a strong double-peak structured feature around 300−350 nm and a second absorption at lower energies (i.e., with its maximun at 528 nm for **1** and 618 nm for **2**). The lowest-energy absorption is largely redshifted in each case, by around 180−200 nm, with respect to the corresponding optical absorption of the unsubstituted *o*-quinoid electron-withdrawing moiety. TDDFT//B3LYP/6-31G** model chemistry predictions nicely agree with the experimental UV−vis features and show that the lowest-energy absorption is due to the one-electron excitation from the HOMO to the LUMO. The DFT topologies of these two frontier molecular orbitals indicate that, whereas the HOMO spreads over the whole CC backbone (with small contributions from the N═C bonds of the fused pyrazine ring in **1** and of the nitrogen atoms of the thiadiaziole ring in **2**), the LUMO is almost exclusively located over the central *o*-quinoid acceptor unit. Consequently, the HOMO → LUMO transition for these narrow band gap co-oligomers implies certain electron-density transfer from the aromatic-like donor thienyl end rings to the central quinoid-like electron-acceptor unit. Calculations show that the band gap lowering in these D−A−D systems, with respect to the homogeneous oligothiophenes, comes not only from the partial stabilization of the LUMO but from a similar destabilization of the HOMO. In addition, TDDFT//B3LYP/6-31G** calculations show that the HOMO → LUMO + 1 excitation of these mixed trimers, which gives rise to their strong visible absorption around 350 nm, is clearly related to the $\pi-\pi^*$ transition in α-linked oligothiophenes and that the topologies of the HOMO and LUMO + 1 in **1** and **2** greatly resemble those of the HOMO and LUMO, respectively, in common oligothiophenes.

The infrared and Raman spectra have been comprehensively assigned with the help of DFT//B3LYP/6-31G** calculations. The vibrational features of the π-conjugated backbone of the two molecules have been identified and compared with those of the nonpolar oligothiophenes. The general frequency downshift of a few characteristic Raman scatterings of the terthienyl spine upon the attachment of a strong electron-withdrawing thiadiazole or pyrazine-fused ring to the central unit of the chain has been explained in terms of a significant softening of the π-conjugated backbone, specially in the case of **2**, induced by the evolution of the molecular structure to a more quinonoid-like pattern.

Acknowledgment. The authors would like to acknowledge the Dirección General de Enseñanza Superior (DGES, MEC, Spain) for support to this investigation through projects BQU2000-1156 and BQU2003-03194. The research was also supported by the Junta de Andalucía (Spain) under Grant FQM-0159. M.C.R.D. is grateful to the MEC for a personal grant.

References and Notes

(1) Roncali, J. *Chem. Rev.* **1992**, *92*, 711.

(2) (a) Sariciftci, N. S.; Smilowitz, L.; Heeger, A. J.; Wudl, F. *Science* **1992**, *258*, 1474. (b) Kraabel, B.; Hummelen, J. C.; Vacar, D.; Moses, D.; Sariciftci, N. S.; Heeger, A. J. *J. Chem. Phys.* **1996**, *104*, 4267.

(3) Havinga, E. E.; ten Hoeve, W.; Wynberg, H. *Polym. Bull.* **1992**, *29*, 119.

(4) Havinga, E. E.; ten Hoeve, W.; Wynberg, H. *Synth. Met.* **1993**, *55*−*57*, 299.

(5) Karikomi, M.; Kitamura, C.; Tanaka, S.; Yamashita, Y. *J. Am. Chem. Soc.* **1995**, *117*, 6791.

(6) Kitamura, C.; Tanaka, S.; Yamashita, Y. *Chem. Mater.* **1996**, *8*, 570.

(7) Bakhshi, A. K.; Ago, H.; Yoshizawa, K.; Tanaka, K.; Yamabe, T. *J. Chem. Phys.* **1996**, *104*, 5528.

(8) Tachibana, M.; Tanaka, S.; Yamashita, Y.; Yoshizawa, K. *J. Phys. Chem. B* **2002**, *106*, 3549.

(9) (a) Kürti, J.; Surján, P. R.; Kertesz, M. *J. Am. Chem. Soc.* **1991**, *113*, 9865. (b) Tanaka, S.; Yamashita, Y. *Synth. Met.* **1993**, *55*−*57*, 1251. (c) Hanack, M.; Schmid, U.; Röhrig, U.; Toussaint, J.-M.; Adant, C.; Bredás, J.-L. *Chem. Ber.* **1993**, *126*, 1487. (d) Ferraris, J. P.; Bravo, A.; Kim, W.; Hrncir, D. C. *J. Chem. Soc., Chem. Commun.* **1994**, 991. (e) Kitamura, C.; Tanaka, S.; Yamashita, Y. *J. Chem. Soc., Chem. Commun.* **1994**, 1585. (f) Akoudad, A.; Roncali, J. *Chem. Commun.* **1998**, 2081.

(10) Sakamoto, A.; Furukawa, Y.; Tasumi, M. *J. Phys. Chem.* **1994**, *98*, 4635.

(11) Yokonuma, N.; Furukawa, Y.; Tasumi, M.; Kuroda, M.; Nakayama, J. *Chem. Phys. Lett.* **1996**, *255*, 431.

(12) (a) Hernandez, V.; Casado, J.; Ramirez, F. J.; Zotti, G.; Hotta, S.; Lopez Navarrete, J. T. *J. Chem. Phys.* **1996**, *104*, 9271. (b) Casado, J.; Hernandez, V.; Hotta, S.; Lopez Navarrete, J. T. *J. Chem. Phys.* **1998**, *109*, 10419. (c) Moreno Castro, C.; Ruiz Delgado, M. C.; Hernandez, V.; Hotta, S.; Casado, J.; Lopez Navarrete, J. T. *J. Chem. Phys.* **2002**, *116*, 10419. (d) Moreno Castro, C.; Ruiz Delgado, M. C.; Hernandez, V.; Shirota, Y.; Casado, J.; Lopez Navarrete, J. T. *J. Phys. Chem. B* **2002**, *106*, 7163.

(13) (a) Casado, J.; Otero, T. F.; Hotta, S.; Hernandez, V.; Ramirez, F. J.; Lopez Navarrete, J. T. *Opt. Mater.* **1998**, *9*, 82. (b) Casado, J.; Hernandez, V.; Hotta, S.; Lopez Navarrete, J. T. *Adv. Mater.* **1998**, *10*, 1258. (c) Casado, J.; Miller, L. L.; Mann, K. R.; Pappenfus, T. M.; Kanemitsu, Y.; Orti, E.; Viruela, P. M.; Pou-Amerigo, P.; Hernandez, V.; Lopez Navarrete, J. T. *J. Phys. Chem. B* **2002**, *106*, 3872. (d) Casado, J.; Miller, L. L.; Mann, K. R.; Pappenfus, T. M.; Hernandez, V.; Lopez Navarrete, J. T. *J. Phys. Chem. B* **2002**, *106*, 3597. (e) Casado, J.; Ruiz Delgado, M. C.; Shirota, Y.; Hernandez, V.; Lopez Navarrete, J. T. *J. Phys. Chem. B* **2003**, *107*, 2637.

(14) Hernandez, V.; Casado, J.; Effenberger, F.; Lopez Navarrete, J. T. *J. Chem. Phys.* **2000**, *112*, 5105.

(15) Gonzalez, M.; Segura, J. L.; Seoane, C.; Martin, N.; Garin, J.; Orduna, J.; Alcala, R.; Villacampa, B.; Hernandez, V.; Lopez Navarrete, J. T. *J. Org. Chem.* **2001**, *66*, 8872.

(16) (a) Zerbi, G.; Castiglioni, C.; Del Zoppo, M. *Electronic Materials: The Oligomer Approach*; Wiley-VCH: Weinheim, 1998; p 345. (b) Castiglioni, C.; Gussoni, M.; Lopez Navarrete, J. T.; Zerbi, G. *Solid State Commun.* **1988**, *65*, 625. (c) Lopez Navarrete, J. T.; Zerbi, G. *J. Chem. Phys.* **1991**, *94*, 957 and 965 (d) Hernandez, V.; Castiglioni, C.; Del Zoppo, M.; Zerbi, G. *Phys. Rev. B* **1994**, *50*, 9815. (e) Agosti, E.; Rivola, M.; Hernandez, V.; Del Zoppo, M.; Zerbi, G. *Synth. Met.* **1999**, *100*, 101.

(17) (a) Ehrendorfer, C.; Karpfen, A. *J. Phys. Chem.* **1994**, *98*, 7492. (b) Ehrendorfer, C.; Karpfen, A. *J. Phys. Chem.* **1995**, *99*, 5341.

(18) Frisch, M. J.; Trucks, G. W.; Schlegel, H. B.; Scuseria, G. E.; Robb, M. A.; Cheeseman, J. R.; Zakrzewski, V. G.; Montgomery, J. A., Jr.; Stratmann, R. E.; Burant, J. C.; Dapprich, S.; Millam, J. M.; Daniels, A. D.; Kudin, K. N.; Strain, M. C.; Farkas, O.; Tomasi, J.; Barone, V.; Cossi,

M.; Cammi, R.; Mennucci, B.; Pomelli, C.; Adamo, C.; Clifford, S.; Ochterski, J.; Petersson, G. A.; Ayala, P. Y.; Cui, Q.; Morokuma, K.; Malick, D. K.; Rabuck, A. D.; Raghavachari, K.; Foresman, J. B.; Cioslowski, J.; Ortiz, J. V.; Stefanov, B. B.; Liu, G.; Liashenko, A.; Piskorz, P.; Komaromi, I.; Gomperts, R.; Martin, R. L.; Fox, D. J.; Keith, T.; Al-Laham, M. A.; Peng, C. Y.; Nanayakkara, A.; Gonzalez, C.; Challacombe, M.; Gill, P. M. W.; Johnson, B. G.; Chen, W.; Wong, M. W.; Andres, J. L.; Head-Gordon, M.; Replogle, E. S.; Pople, J. A. *Gaussian 98*, revision A.7; Gaussian, Inc.: Pittsburgh, PA, 1998.

(19) Becke, A. D. *J. Chem. Phys.* **1993**, *98*, 1372.

(20) Stephens, P. J.; Devlin, F. J.; Chabalowski, F. C. F.; Frisch, M. J. *J. Phys. Chem.* **1994**, *98*, 11623.

(21) Novoa, J. J.; Sosa, C. *J. Phys. Chem.* **1995**, *99*, 15837.

(22) Scott, A. P.; Radom, L. *J. Phys. Chem.* **1996**, *100*, 16502.

(23) Rauhut, G.; Pulay, P. *J. Phys. Chem.* **1995**, *99*, 3093.

(24) Francl, M. M.; Pietro, W. J.; Hehre, W. J.; Binkley, J. S.; Gordon, M. S.; Defrees, D. J.; Pople, J. A. *J. Chem. Phys.* **1982**, *77*, 3654.

(25) (a) Runge, E.; Gross, E. K. U. *Phys. Rev. Lett.* **1984**, *52*, 997. (b) Gross, E. K. U.; Kohn, W. *Adv. Quantum Chem* **1990**, *21*, 255. (c) *Density Functional Theory*, Gross, E. K. U.; Driezler, R. M., Eds.; Plenum Press: New York, 1995; p 149.

(26) Casida, M. E. *Recent Advances in Density Functional Methods, Part I.*; Chong, D. P., Ed.; World Scientific: Singapore, 1995; p 115.

(27) Koch, W.; Holthausen, M. C. *A Chemist's Guide to Density Functional Theory;* Wiley-VCH: Weinheim, 2000.

(28) Tanaka, S.; Yamashita, Y. *Synth. Met.* **1995**, *69*, 599.

(29) Casado, J.; Pappenfus, T. M.; Miller, L. L.; Mann, K. R.; Orti, E.; Viruela, P. M.; Pou-Amerigo, R.; Hernandez, V.; Lopez Navarrete, J. T. *J. Am. Chem. Soc.* **2003**, *125*, 2524.

(30) Marder, S. R.; Gorman, C. B.; Meyers, F.; Perry, J. W.; Bourhill, G., Brédas, J.-L.; Pierce, B. M. *Science* **1994**, *265*, 632.

(31) Marder, S. R.; Perry, J. W.; Tiemann, B. G.; Gorman, C. B.; Gilmour, S.; Biddle, S. L.; Bourhill, G. *J. Am. Chem. Soc.* **1993**, *115*, 2524.

(32) Bourhill, G.; Brédas, J.-L.; Cheng, L.-T.; Marder, S. R.; Meyers, F.; Perry, J. W.; Tiemann, B. G. *J. Am. Chem. Soc.* **1994**, *116*, 2619.

(33) Raimundo, J. M.; Blanchard, P.; Ledoux-Rak, I.; Hierle, R.; Michaux, L.; Roncali, J. *Chem. Commun.* **2000**, 1597.

(34) Radeglia, R.; Dähne, S. *J. Mol. Struct.* **1970**, *5*, 399.

(35) Tanaka, S.; Tomura, M.; Yamashita, Y. *Heterocycles* **1994**, *37*, 693.

(36) Daminelli, G.; Widany, J.; Di Carlo, A.; Lugli, P. *J. Chem. Phys.* **2001**, *115*, 4919.

(37) Zerbi, G. *Handbook of Conducting Polymers*; Skotheim, T. A., Elsenbaumer, R. L., Reynolds, J. R., Eds.; Marcel Dekker: New York, 1998.

(38) Ruiz Delgado, M. C.; Hernandez, V.; Casado, J.; Lopez Navarrete, J. T.; Raimundo, J.-M.; Blanchard, P.; Roncali, J. *Chem.*−*Eur. J.* **2003**, *9*, 3670.

(39) Harada, I.; Furukawa, Y. *Vibrational Spectra and Structure*; Durig, J., Ed.; Elsevier: Amsterdam, 1981; Vol. 19, p 369.